



**HAL**  
open science

# Connectivity, permeability and channeling in randomly-distributed and kinematically-defined discrete fracture network models

Julien Maillot, Philippe Davy, Romain Le Goc, Caroline Darcel, Jean-Raynald De Dreuzy

► **To cite this version:**

Julien Maillot, Philippe Davy, Romain Le Goc, Caroline Darcel, Jean-Raynald De Dreuzy. Connectivity, permeability and channeling in randomly-distributed and kinematically-defined discrete fracture network models. *Water Resources Research*, 2016, 52 (11), pp.8526-8545. 10.1002/2016WR018973 . insu-01381214

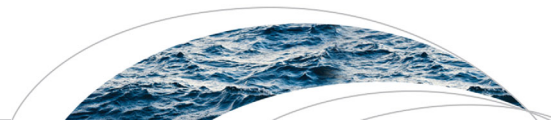
**HAL Id: insu-01381214**

**<https://insu.hal.science/insu-01381214>**

Submitted on 14 Nov 2016

**HAL** is a multi-disciplinary open access archive for the deposit and dissemination of scientific research documents, whether they are published or not. The documents may come from teaching and research institutions in France or abroad, or from public or private research centers.

L'archive ouverte pluridisciplinaire **HAL**, est destinée au dépôt et à la diffusion de documents scientifiques de niveau recherche, publiés ou non, émanant des établissements d'enseignement et de recherche français ou étrangers, des laboratoires publics ou privés.



## RESEARCH ARTICLE

10.1002/2016WR018973

### Key Points:

- Connectivity of Poisson models is greater than mechanical models
- Permeability of kinematically defined model is lower than Poisson models
- For the kinematically defined models, flow channeling is lower than Poisson models

### Correspondence to:

P. Davy,  
philippe.davy@univ-rennes1.fr

### Citation:

Maillot, J., P. Davy, R. Le Goc, C. Darcel, and J.R. de Dreuzy (2016), Connectivity, permeability, and channeling in randomly distributed and kinematically defined discrete fracture network models, *Water Resour. Res.*, 52, doi:10.1002/2016WR018973.

Received 23 MAR 2016

Accepted 9 OCT 2016

Accepted article online 13 OCT 2016

# Connectivity, permeability, and channeling in randomly distributed and kinematically defined discrete fracture network models

J. Maillot<sup>1,2</sup>, P. Davy<sup>1</sup>, R. Le Goc<sup>2</sup>, C. Darcel<sup>2</sup>, and J.R. de Dreuzy<sup>1</sup>

<sup>1</sup>Géosciences Rennes, UMR CNRS 6118, Université de Rennes1, Rennes, France, <sup>2</sup>ITASCA Consultants SAS, Ecully, France

**Abstract** A major use of DFN models for industrial applications is to evaluate permeability and flow structure in hardrock aquifers from geological observations of fracture networks. The relationship between the statistical fracture density distributions and permeability has been extensively studied, but there has been little interest in the spatial structure of DFN models, which is generally assumed to be spatially random (i.e., Poisson). In this paper, we compare the predictions of Poisson DFNs to new DFN models where fractures result from a growth process defined by simplified kinematic rules for nucleation, growth, and fracture arrest. This so-called “kinematic fracture model” is characterized by a large proportion of T intersections, and a smaller number of intersections per fracture. Several kinematic models were tested and compared with Poisson DFN models with the same density, length, and orientation distributions. Connectivity, permeability, and flow distribution were calculated for 3-D networks with a self-similar power law fracture length distribution. For the same statistical properties in orientation and density, the permeability is systematically and significantly smaller by a factor of 1.5–10 for kinematic than for Poisson models. In both cases, the permeability is well described by a linear relationship with the areal density  $p_{32}$ , but the threshold of kinematic models is 50% larger than of Poisson models. Flow channeling is also enhanced in kinematic DFN models. This analysis demonstrates the importance of choosing an appropriate DFN organization for predicting flow properties from fracture network parameters.

## 1. Introduction

In crystalline rocks and sedimentary layers with low matrix porosity, most, if not all, flow takes place within fractures, and the fracture network constitutes the basic structure that defines both permeability and flow path organization. Thus predicting both, which is required for groundwater management or environmental risk assessment, is intimately related to our ability to provide pertinent models of fracture networks. A modeling strategy basically consists in generating 3D fracture networks with the statistical properties derived from field observations [Cacas *et al.*, 1990a, 1990b; Cvetkovic *et al.*, 2004; Dershowitz and Einstein, 1988; Follin *et al.*, 2013; Jing and Stephansson, 2007]. This discrete fracture network (DFN) approach, which is widely used to generate equivalent media, is complementary to continuum heterogeneous approaches [de Dreuzy *et al.*, 2012; Hsieh, 1998; Long *et al.*, 1982; Neuman, 2005; Selroos *et al.*, 2002] and allows for a better integration of geological data into flow models [Follin *et al.*, 2013].

The difficulty is on the one hand that fractures are complex objects, ubiquitous at all scales, and on the other hand that direct observations of fracture networks are relatively scarce, since limited to surface outcrops, tunnel wall, and core drilling. A big challenge is to find DFN statistical models that are universal enough to be inferred from measures made at a few (small) local places and extrapolated to the rest of the 3-D domain. Upscaling statistical distribution at large scale and for large fractures is in particular a fundamental issue that has been addressed by several studies [Crampin, 1999; Davy *et al.*, 2006; Turcotte, 1986]. The importance of fracture density, orientation, length, and transmissivity distributions has been extensively assessed [de Dreuzy *et al.*, 2001a, 2001b, 2002, 2012; Erhel *et al.*, 2009b; Margolin *et al.*, 1998; Park *et al.*, 2001]. But only a few studies address the issue of spatial correlations—thus of the details of fracture network organization—although they are potentially of great importance for flow [Darcel *et al.*, 2003; Davy *et al.*, 2010]. Most of the studies based on a DFN description of fracture networks (references cited above)

assume that fractures are randomly placed into the studied domain given a certain density. This assumption is referred thereafter as the Poisson model (PM).

In this paper, we aim at testing an advanced DFN model, which mimics the growth of fractures with simplified kinematic rules of nucleation, growth, and arrest [Davy *et al.*, 2010, 2013]. The model successfully describes two striking properties of natural fracture systems clearly important for connectivity and flow:

1. the large occurrence of T intersections (a fracture ends up on another), which is a significant difference with Poisson models;
2. the power law distribution of fracture lengths, which naturally emerges from the growth and arrest rules (as it should do in natural fracture systems).

These models are further named “kinematic fracture models” (KFM) since they provide a kinematic history of fractures (see next section); they are compared with their equivalent “Poisson” models (PM) (with same fracture density, same length and orientation distributions, but different organization) to test the importance of fracture organization.

The study is performed for 3-D fracture networks, for which efficient numerical methods have only been recently developed [Erhel *et al.*, 2009b], but in which only very few investigations have yet been performed [see, however, de Dreuzy *et al.*, 2012; Wellman *et al.*, 2009]. Hydraulic properties are calculated for simplified models of transmissivity distributions per fracture: constant, lognormal with varying standard deviation, and in both cases, a single transmissivity value per fracture.

We pay a special attention to flow localization/channeling issues, which is known to be a characteristic of fractured aquifer [Martinez-Landa and Carrera, 2005; Tsang and Neretnieks, 1998]. The capacity of DFN models to reproduce flow channeling is essential to accurately estimate the hydraulic properties [Kerrou *et al.*, 2008; Ronayne and Gorelick, 2006; Trinchero *et al.*, 2008].

This paper is organized as follows. First, the DFN kinematic and Poisson models are described, as well as indicators and metrics used to characterize the flow properties. Second, we present results about the geometry and connectivity properties of DFN models. Third, we present results on flow properties calculated by assuming a constant transmissivity throughout all fractures; in this case, the permeability reveals the effective connectivity properties of the medium [de Dreuzy *et al.*, 2001a; Renshaw, 1999]. Last, we analyze the hydraulic properties calculated with a lognormal transmissivity distribution and different log standard deviation. Widening the transmissivity distribution favors channeling, but may either enhance or reduce the bulk permeability, depending on the fracture network structure [de Dreuzy *et al.*, 2010; Desbarats, 1992; Knudby and Carrera, 2005; Ronayne and Gorelick, 2006; Scheibe and Yabusaki, 1998].

## 2. Models and Methods

The DFN method is a discrete approach where the geological medium is approximated by a network of fractures, on which flow and mechanical properties are calculated [Long *et al.*, 1982]. Considering the difficulty to get an exhaustive description of fractures, DFN is built from a statistical description of fracture properties (size, orientations, aperture, etc.) and generally within the Poisson hypothesis, which assumes that fractures are independent of each other [Berkowitz, 1995, 2002; Cacas *et al.*, 1990a, 1990b; Jing and Stephansson, 2007; Long *et al.*, 1985; Long and Billaux, 1987; McClure and Horne, 2013].

### 2.1. Poisson Models

The term “Poisson” refers to the Poisson distribution, which describes the distribution of a set of elements randomly distributed in a volume [Poisson, 1837]. Here the distribution applies to the position of the fracture centers under a known bulk density (number of elements per unit volume). Fractures are thus elements considered independent of each other. These models have been studied theoretically with lognormal fracture size distribution [Andersson and Dverstorp, 1987; Cacas *et al.*, 1990a; Long and Billaux, 1987], or power laws [Bour *et al.*, 2002; Davy *et al.*, 1990; Davy, 1993; Gudmundsson, 1987; Odling, 1997; Scholz and Cowie, 1990; Segall and Pollard, 1983].

## 2.2. Kinematic DFN Models

Although convenient, the Poisson hypothesis is clearly inconsistent with some basic characteristics of fracture networks, such as the large number of T intersections [Hardebol *et al.*, 2015; Sanderson and Nixon, 2015], and it is not yet clear if this affects the ability of Poisson models to predict flow in fracture networks. To challenge this question, we use a recent DFN methodology developed by Davy *et al.* [2010, 2013], which both mimics geological fracturing processes, and allows for fast and simple stochastic simulations. In this approach, fracture networks are generated in a three-stages process: nucleation of initial cracks, fracture growth, and arrest. This “life cycle” involves processes at the fracture scale (e.g., stress enhancement and damaging at the fracture tips), as well as interactions between concurrently growing fractures that eventually lead to stopping fracture growth on “T” configurations. These models naturally produce, from very few kinematic rules inspired from mechanical considerations, the widely observed power law length distributions for both fault and joint networks [Bonnet *et al.*, 2001]. We refer to both original papers for a complete description of the model, and of its capacity to generate networks with realistic properties. We only give below a short summary.

The first stage of this kinematic model is nucleation, which is assumed to be a random process defined by a distribution of nuclei positions, orientations and lengths, and a nucleation rate  $\dot{n}_N = \frac{dn_N}{dt}$ , where  $n_N$  is the number of nuclei per unit volume. Once created, a fracture grows at a rate defined by Charles’ law [Atkinson and Meredith, 1987; Charles, 1958]:

$$\frac{dl}{dt} = Cl^a, \quad (1)$$

where  $l$  is the fracture length,  $C$  the growth rate, and  $a$  is the growth exponent. Without a limit to this growth process, the growth regime eventually leads to a power law density distribution of fracture sizes such that:

$$n(l) = \frac{\dot{n}_N}{C} \cdot l^{-a}, \quad (2)$$

where  $n(l)dl$  is the number of fractures per unit volume, whose size is in the range  $[l, l+dl]$ .

Davy *et al.* [2010] demonstrate that, although complex, the arrest process is dominated by a hierarchical rule, where the large fractures can stop smaller ones, while the reverse is unlikely. Such rule obviously simplifies the mechanical reasons for stopping fracture growth, but it roughly describes the main mechanical interactions between fractures, and it is statistically consistent with the large number of commonly observed T-like fracture intersections. The fracture arrest rule potentially occurs after hitting the first larger fracture (mode A with one “T” termination maximum per fracture), or it continues in the opposite direction of the first intersection until it intersects a second larger fracture (mode B with two “T” terminations maximum per fracture). This arrest rule leads to a quite universal fracture density distribution:

$$n(l) = \alpha \cdot l^{-(D+1)}, \quad (3)$$

where  $D$  is the dimension of the DFN (here  $D = 3$ ) and  $\alpha$  a density term that depends on the fracture orientation distribution and the details of the arrest rule (mode A or B, see above) [Davy *et al.*, 2013].

A fracture is in a growing state (equation (1), and eventual distribution described by equation (2)) when its size remains smaller than the distance to others. Thus equation (2) statistically characterizes a *sparse* network of small unconnected fractures. In contrast, arrested fractures form a network of connected fractures, whose density given by equation (3) is the largest one that can be obtained with these models. The eventual length distribution depends on the generation time, and thus on the total number of generated fractures. Equation (3) is the eventual length distribution if the process is continued up to the point where all fractures are arrested. Before this limit, there is a transition scale between the *sparse* and *dense* regime, which corresponds to a critical length scale  $l_c$ . This transition scale is also a connectivity scale, which decreases during the network growth. Davy *et al.* [2010] showed from an analysis of the percolation parameter (see also below) that the *sparse* regime should have little effect on permeability.

In addition to the arrest mode (A or B), the nature of the growth regime (ratio  $C/\dot{n}_N$ ) is critical to the eventual dense regime structure. If  $C$  is much larger than  $\dot{n}_N$ , the time for a fracture to grow is short compared

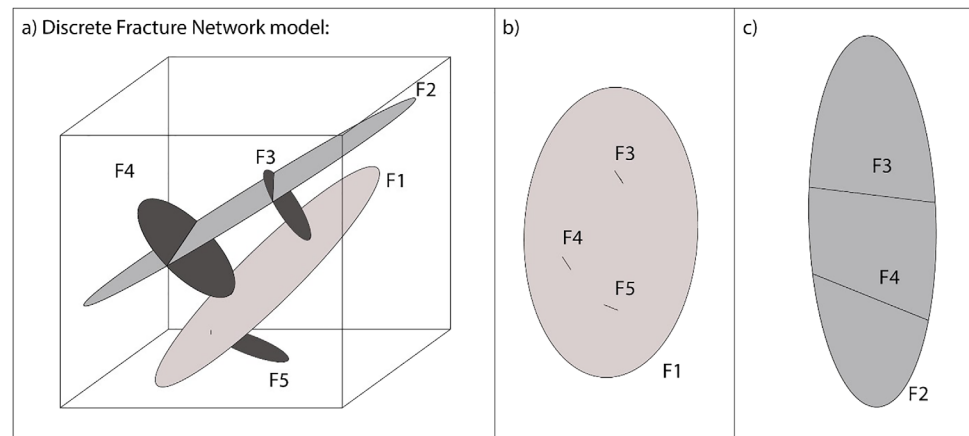


**Figure 1.** (a) schematic 3-D representation of five fractures of the total DFN. (b) In-plane representation of the largest fracture F1 (see Figure 1a), and its intersection with F3, F4, and F5. All the intersections in F1 are of T-type, meaning that F3, F4, and F5 are smaller fractures that abut on it. (c) In-plane representation of the fracture F2, and intersections with F3 and F4. All the intersections in F2 are of X-type, meaning that F3 and F4 are smaller fractures that were cut through during the growth of F2.

with the time between the appearance of successive nuclei. Thus fractures grow one by one in a sequential mode, and most of the intersections are of “T” type. In contrast, if  $C$  is smaller than  $\dot{n}_N$ , a large number of fractures grow concomitantly, which produces a large number of “X” intersections when a larger fracture intersects a smaller one. The former growth mode will be called thereafter sequential (S), the latter competitive (C).

The possibility to contain both “T” and “X” intersections is one main characteristic of these kinematic models. On the contrary, Poisson models have only “X” intersections. When large fractures grow through smaller ones “X” intersections are created while “T” intersections are created when small fractures are arrested by larger ones. A representation of both types of intersections is given in Figure 1. Changing the parameters of arrest mode, nucleation, and growth will therefore lead to different geometrical structures.

### 2.3. Selected Models and Parameters

The study is performed in 3-D with disk-shaped fractures. For the kinematic model, we limit the present analysis to the dense regime (above  $l_c$ ). Over that range, all fractures are arrested and thus connected at least to another one. The sparse regime contribution (below  $l_c$ ), where fractures are statistically not connected, is not analyzed further in this study. As a consequence, the present analysis relies on one single power law model of exponent  $-4$  for the fracture size distribution and also on several different spatial structures and densities. The density term  $\alpha$  is related to details of the kinematic model rules and DFN spatial structure. Several kinematic models are defined, of arrest mode A or B and growth mode C or S, leading to four kinematic fracture model variations named KFMAS, KFMAC, KFMBBS, and KFMBBC. For the four models:

1. As in Davy *et al.* [2013], we assume that nuclei are randomly distributed in position with a uniform probability in the generation domain. More sophisticated models will be developed in a future work to take account of the distribution of stresses around fractures [Bonneau *et al.*, 2016].
2. The initial nuclei pole orientation distribution is isotropic and so is the final DFN pole orientation distribution [Davy *et al.*, 2013].
3. The initial nuclei length distribution is a tight power law with a very small exponent of  $-5$ .
4. The growth law parameters are  $C=1$  and  $a=3$  (equation (2)). The difference between sequential and competitive models is obtained by changing the nucleation rate.
5. The T-intersection size is taken constant as  $1/20$  of the minimum fracture size.
6. The ratio between the smallest fracture and the system size is at least equal to 10. This range is large enough to give a permeability independent of  $L$  (in other words,  $L$  is larger than the Representative Elementary Volume [Long *et al.*, 1982]).

For all networks, we assume that the transmissivity within each fracture is constant. *de Dreuzy et al.* [2012] have studied the effect of a distribution of apertures within a fracture, and shown that it can be replaced by a single transmissivity value for each fracture if the system size is larger than about 20 times the correlation length of aperture variation. We assume that this hypothesis applies to the studied DFN. Transmissivity can vary from one fracture to another. In this study, we assume that the transmissivity per fracture follows a log-normal distribution, whose log standard deviation  $\sigma$  varies from 0 (section 4, where transmissivities are constant) up to 2 (section 5).

For each kinematic model, an equivalent Poisson model is defined, with the same density, size, and orientation distributions. They differ only in the spatial structure (random fracture positions in the Poissonian hypothesis, and arising from the interactions between fractures in this kinematic approach).

#### 2.4. DFN Metrics

The DFN metrics listed in this section refer to both geometrical and effective hydraulic properties quantities.

The connectivity properties of power law distributed Poisson models have been intensively studied by *Bour and Davy* [1997, 1998], *de Dreuzy et al.* [2000], and *Nakaya and Nakamura* [2007]. It was demonstrated that the exponent of the length distribution is critical for determining how the different classes of fracture length participate in the bulk connectivity. An exponent of  $-4$ , as it is here (equation (3)), is precisely the limit between systems controlled by the largest fractures (exponents larger than  $-4$ ) and systems controlled by the smallest, for which percolation theory applies (exponents smaller than  $-4$ ). For exponent equal to  $-4$ , all logarithmic classes of fracture length contribute equally to percolation [*Bour and Davy*, 1998]. In any case, a relevant metrics to quantify the connectivity is the percolation parameter defined as:

$$p = \int_l \frac{\pi^2}{8} l^3 n(l) dl = \frac{1}{V} \sum_f \frac{\pi^2}{8} l_f^3, \quad (4)$$

where  $V$  is the volume of the studied system, and  $l_f$  the length of fracture  $f$ .

For 3-D random disks, bulk connectivity is obtained when the percolation parameter is larger than a threshold value  $p_c = 2.5$  [*de Dreuzy et al.*, 2000].

A second DFN geometrical metrics is the total fracture surface per unit volume. It is often named  $p_{32}$  [*Der-showitz and Herda*, 1992]:

$$p_{32} = \frac{1}{V} \sum_f A_f = \frac{1}{V} \sum_f \frac{\pi}{4} l_f^2, \quad (5)$$

where  $A_f$  is the area of the fracture  $f$ .

$p_{32}$  is the density term that controls permeability for dense networks, where effective medium theory applies [*de Dreuzy et al.*, 2000; *Kirkpatrick*, 1973; *Oda*, 1985].

In addition, the following flow global metrics will be defined and used in the analyses:

1. The bulk DFN permeability  $K$  calculated for a distribution of fracture transmissivities—the special case when all fracture transmissivities are constant is called the effective connectivity.
2. The backbone density  $d_b$  defined as the structure that carries flow [*Stauffer and Aharony*, 1992]. A more complete definition is given in the section 4.3.
3. The flow channeling density indicator  $d_Q$ , which reflects the portion of the total fracture surface where flow is significant [*Le Goc et al.*, 2010].  $d_Q^{-1}$  is also a measure of the distance between the main flow paths, directly comparable with borehole flow measurements. A complete definition of  $d_Q$  is given in the section 4.4. Note that  $d_Q$  takes into account the flow intensity, while  $d_b$  does not.
4. The power-average exponent  $\omega$ , which quantifies the way permeability averages a transmissivity distribution.  $\omega$  varies between  $-1$  (harmonic averaging, when fractures are connected in series) and  $1$  (arithmetic averaging, when fractures are in parallel).  $\omega$  is thus a measure of the flow structure organization (see section 5).

### 2.5. Dimensional Considerations

This study aims at being as generic as possible with results applicable to DFN systems whatever their absolute size and absolute permeability. The DFN models parameters are therefore expressed as dimensionless quantities, which allows for their generalization to any equivalent system. In this section, we develop the dimensional analysis.

In general, the system permeability is defined from a set of fracture transmissivities  $\{T_i\}$ , lengths  $\{l_i\}$ , and position coordinates  $\{\mathbf{x}_i\}$  ( $3N$  parameters, if  $N$  is the total number of fractures in the system). For the scaling analysis, we need only two basic parameters: a characteristic transmissivity of fracture  $T_o$ , and a characteristic length scale  $l_o$ ; the characteristic permeability is deduced from the two others ( $K_o = T_o/l_o$ ). The main dimensionless variables write as  $K^* = K/K_o$ ,  $T^* = T/T_o$ ,  $l^* = l/l_o$ ,  $\mathbf{x}^* = \mathbf{x}/l_o$ ,  $p_{32}^* = p_{32}l_o$ , etc. Two systems have the dimensionless permeability  $K^*$  if the fractures characteristics  $\{T_f^*\}$ ,  $\{l_f^*\}$ , and  $\{\mathbf{x}_f^*\}$  are identical. In a statistical analysis, we replace these three distributions by the distribution parameters. In this study, the distribution parameters are:

1. The fracture transmissivity distribution  $\{T_f\}$  is characterized by a set of statistical parameters that describe the mean, variability, and more if necessary. In the case of lognormal transmissivity distributions, two parameters are necessary, the log-average transmissivity  $T_m$ , and the dimensionless log-variability  $\sigma$ ;
2. The fracture length distribution  $\{l_f\}$  is a power law defined by the smallest fracture size  $l_m$ , the largest fracture size  $l_M$ , the exponent of the power law distribution  $a$ , and the density term  $\alpha$ . Note that if  $l_M$  is much larger than the system size  $L$ ,  $l_M$  has almost no influence on the system permeability.
3.  $\{\mathbf{x}_f\}$  is a set of position coordinates within the system (cube of edge size  $L$ ), according to a position model (randomly distributed for the Poisson model, and distributed differently for the kinematic models).

From the previous description, the only significant scales here are the smallest fracture  $l_m$ , and the log-averaged transmissivity  $T_m$ . We thus use both as the characteristic length ( $l_o = l_m$ ) and transmissivity ( $T_o = T_m$ ). The system is also characterized by three other dimensionless parameters: the density  $\alpha$  and power exponent of the length distribution, and the log-variability of fracture transmissivity  $\sigma$ .

Written in dimensionless variables, the smallest fracture length is (by definition)  $l_m^* = 1$ , and the system size is  $L^* = \frac{L}{l_o} = 10$ . For the ease of reference, all of the below figures and tables are written with dimensionless values parameter values.

### 2.6. Numerical Method

Fractures networks are generated using the assumptions and methodology defined in 2.2 with the new self-standing UFMLAB software. Flows are determined with the conformal mixed-hybrid finite element methods implemented in the development platform H2OLAB [Erhel et al., 2009a]. More details about the platform and its availability can be found in the website <http://h2olab.inria.fr/>.

For all models, DFN are generated in a cubic volume of edge size  $L_G = 15$  (volume  $V = 15^3$ ). The geometrical and hydraulic analyses are performed in a cubic subdomain of size  $L = 10$  to avoid boundary effects. In addition, kinematic models are built from nuclei of minimum size 0.5, while the studied DFN are defined after removal of fractures smaller than  $l_{\min} = 1$  (i.e., whose length is close to nuclei sizes). For all models, fracture sizes thus range over 1 order of magnitude between  $l_{\min} = 1$  and  $L = 10$ .

The steady state flow equation  $\nabla(T\nabla h) = 0$  is applied in the fractures where  $h$  is the hydraulic head, and  $T$  is the local transmissivity. As already mentioned in section 2.3, the transmissivity within each fracture is taken constant or lognormally distributed. Permeameter-like boundary conditions are applied: hydraulic heads are fixed at  $h = 1$  and  $h = 0$  on the two opposite faces  $x^+$  and  $x^-$  of the cubic system, while impervious conditions are applied to the other cube faces. The flow equation is solved with a mixed-hybrid finite element scheme applied on a conformal triangular mesh [Erhel et al., 2009a]. Fracture intersections smaller than the mesh resolution are removed from the flow domain. Mesh resolution is set 10 times larger than the smallest fracture length, and larger than T intersections. Only minor X intersections are effectively removed without any significant modifications of the connectivity and effective permeability. Simulations are performed with algebraic multigrid solvers that can manage thousands of fractures on PC-computers with large RAM memory [De Dreuzy et al., 2013]. For each of the 8 DFNs (4 KFM and 4 PM), statistics are obtained over a minimum of 1000 Monte-Carlo realizations.

**Table 1.** Main Geometrical Characteristics of Inematic (KFM) and Equivalent Poisson (PM) Models<sup>a</sup>

Kinematic Models	KFMAS	KFMAC	KFMBS	KFMBC
$\dot{n}_N$ (nucleation rate during growth)		Competitive model: 81,000 Sequential model: 810		
$\alpha$	2.1	2.6	3.4	3.5
$p_{32}$	1.59 ( $\pm 0.029$ )	1.89 ( $\pm 0.033$ )	2.59 ( $\pm 0.037$ )	2.68 ( $\pm 0.041$ )
$p$ (percolation parameter)	5.98 ( $\pm 0.56$ )	7.68 ( $\pm 0.63$ )	10.2 ( $\pm 0.62$ )	11.39 ( $\pm 0.77$ )
$n_F$ (number of fractures)	811 ( $\pm 21$ )	840 ( $\pm 21$ )	1238 ( $\pm 23$ )	1146 ( $\pm 24$ )
$n_I$ (number of intersection)	712 ( $\pm 25$ )	1140 ( $\pm 38$ )	2534 ( $\pm 62$ )	2649 ( $\pm 64$ )
$T$ (% of T intersections)	94%	66%	92%	74%
Equivalent Poisson Models	PMAS	PMAC	PMBS	PMBC
All other parameters are identical to kinematic models				
$n_I$ (number of intersections)	1481 ( $\pm 92$ )	2094 ( $\pm 117$ )	3908 ( $\pm 180$ )	4170 ( $\pm 190$ )
$T$ (% of T intersections)			0%	

<sup>a</sup>Mode A (B, resp.) correspond to kinematic models where growth is defined by one (two, resp.) degree(s) of freedom. C (S, resp.) designs competitive (sequential, resp.) model.

### 3. DFN Geometry and Connectivity Properties

#### 3.1. Density Parameters

The main geometrical characteristics of DFN models are summarized in Table 1. As predicted by equation (3), all kinematic models are well fitted by a power law with an exponent  $-4$  (see the length distributions kinematic and Poisson DFN models plots in Figure 2). The dimensionless density term  $\alpha$ , given in Table 1, varies from 2.1 to 3.5 according (i) to the arrest rule—mode B with potentially 2 T-terminations per fracture have a higher density than mode A with 1-T per fracture—and (ii) to the growing mode, where the density of sequential growth is smaller than of competitive one. The equivalent Poisson models are generated from the parameters of the kinematic model power law fits. The differences between kinematic (blue points) and Poisson (red points) models are very small, between 1.5% and 6%.

The total number of fractures varies between 800 and about 1200 depending on models. The average of the main properties of DFNs is presented in the Table 1. The differences in  $p_{32}$  reflect the differences in  $\alpha$  discussed above with mode-B models 40–60% higher than mode-A ones, and a difference of 23% maximum between sequential (S) and competitive (C) modes. For all DFNs, the percolation parameter  $p$  is significantly larger than the percolation threshold  $p_c$  estimated at  $p_c \sim 2.5$  for Poisson disks with power law length distribution [de Dreuzy et al., 2000]. Note that a similar percolation threshold has been obtained for the kinematic models by removing fractures one by one until disconnection.

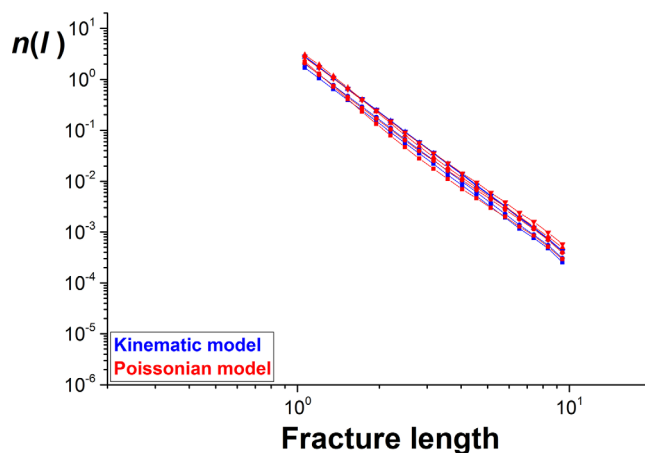


**Figure 2.** Density distribution of fracture sizes (i.e., number of fractures per unit volume). The four kinematic models and their equivalent Poisson models are drawn with different colors (see legend).

#### 3.2. Connectivity

The total number of intersections is also controlled by the arrest mode, with 2–3.5 times more intersections in mode B than in mode A, while it increases of 5–40% for type C compared with type S. An important difference between modes C and S is the nature of intersections. S models produces significantly more T intersections ( $>90\%$  of T) than C models (66–74% of T).

Although the fracture distribution characteristics (length, orientation, density, and number) are similar between Poisson and kinematic models, the connectivity is very different with 1.6–2 times more intersections in Poisson than in Kinematic DFN (Table 1). This is further investigated in the next section.

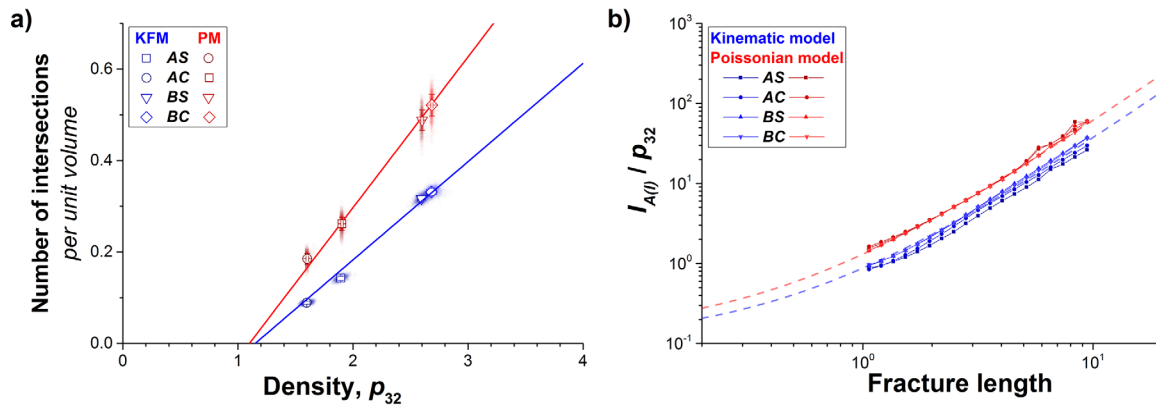


**Figure 3.** (a) Number of intersection normalized by the domain volume, as a function of the fracture density  $p_{32}$ . (b) Number of intersections per fracture ( $I_f$ ) normalized by the mass density  $p_{32}$  as a function of fracture length. The Poisson models are symbolized in red and the kinematic models in blue. The dashed lines represent the theoretical equation developed in the Appendix A with  $\beta=0.85$  (red curve, PM models), or  $\beta=0.45$  (blue curve, KFM models).

The number of intersections is controlled by linear relations of the form  $N_i = k(p_{32} - d_c)$  (Figure 3a), where  $d_c \sim 1.1$  is likely the density at connectivity threshold. The  $k$  term differs between models:  $k=0.33$  for Poisson models, and  $k=0.215$  for kinematic models (Figure 3a). As a consequence, the difference between both models increases with fracture density.

The number of intersections per fracture  $I_f$  is another proxy for connectivity, which is basic to calculate excluded volumes [Balberg, 1985; Balberg et al., 1984]. For Poisson models,  $I_f(l)$  is an increasing function of  $l$  proportional to the bulk fracture density  $p_{32}$  (see Appendix A). This is verified in the Figure 3b, with all Poissonian models matching the expected theoretical relationship when normalized by  $p_{32}$ . The kinematic models show the same trend as Poisson, but with two main differences: (1) whatever the fracture length, the ratio  $\frac{I_f(l)}{p_{32}}$  is about 2 times lower for kinematic than for Poisson models, and (2) all the kinematic models cannot be described by a single curve although the differences are quite small.

Last, we analyze the percentage of T intersections, which is a typical characteristic of the kinematic models. Figure 4 shows that it is about independent of the fracture length even if a slight increase can be observed for the largest fractures. The largest percentage of T intersections ( $\geq 90\%$ ) is for both sequential models, where only one (or a couple of) fracture(s) can grow at the same time. For competitive models, the T intersections represent 60% (mode A) to 75% (mode B) of the total (see Table 1 for details).

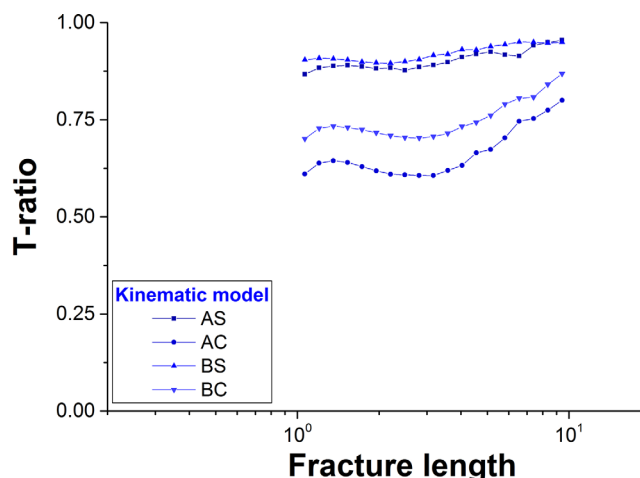


**Figure 4.** Ratio of T intersections per fracture for the four kinematic models.

## 4. Hydraulic Properties at Constant Fracture Transmissivity

### 4.1. Equivalent Permeability

We first calculate the effective connectivity, i.e., the system permeability of fracture networks when all fractures have the same transmissivity  $T_f$  [de Dreuzy et al., 2001a, 2001b; Renshaw, 1999]. For Poisson models well above percolation threshold, the equivalent permeability  $K_{eq}$  should be well described by effective-medium theories [Kirkpatrick, 1973], leading to a linear increase of  $K_{eq}$  with  $p_{32}$ .

$$K_{eq} = k(p_{32} - p_{Qc}), \quad (6)$$

where  $k$  is a constant related to boundary conditions and fracture orientations,

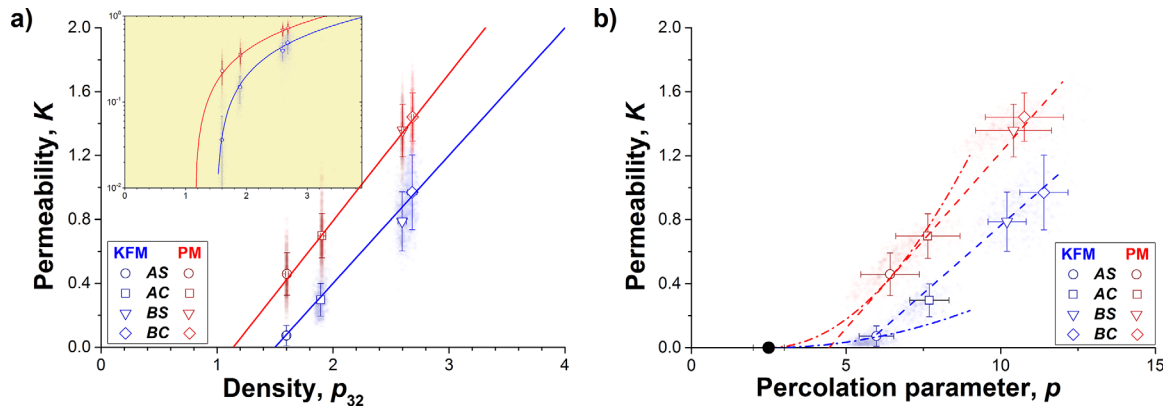


**Figure 5.** (a) Permeability  $K_{eq}$  versus  $p_{32}$  for all studied models; the yellow box shows same data with a logarithmic axis for permeability. (b) Permeability versus percolation parameter for all models; the black dot indicates the percolation threshold. For both graphs, the kinematic models are in blue and their equivalent Poisson models in red. Straight dashed lines are linear fits (see text). Dot-dash lines in the left graph are quadratic fits inspired from the percolation theory. The transparency symbols stand for each DFN simulation, and the large empty symbols represent the property averages for each model.

and  $k \cdot p_{Qc}$  reflects the density of nonactive fractures. Note that this expression is given in dimensionless variables. According to the section 2.5, the “real” permeability is obtained by multiplying  $K_{eq}$  by  $T_f/l_{min}$ , and by dividing  $p_{32}$  by  $l_{min}$ .

As shown in Figure 5a, equation (6) applies on both Poisson and kinematic models, but with different parameters: for PM,  $k=0.46$  and  $p_{Qc}=1.14$ ; for KFM,  $k=0.4$  and  $p_{Qc}=1.5$ . Since the  $k$  parameter is slightly different for both models, their difference in permeability between both models seems to slightly increase with density. For AS, the kinematic model close to percolation threshold, the difference with the equivalent Poisson model reaches a ratio of 10 on average, and even more for some realizations (see the log-lin plot inserted in Figure 5a). For the models with larger density, the ratio between PM and KFM is about 1.4.

Close to the percolation threshold (represented by a black dot in Figure 5b), the permeability should vary as a quadratic relationship  $K \sim (p-p_c)^\mu$  with  $p_c \cong 2.5$  and  $\mu \cong 2$  in 3-D [Mitiescu and Musolf, 1983; Stauffer and Aharony, 1992]. Figure 5b shows the relationship between permeability and percolation parameter for both models, with quadratic (dash-dot lines) and linear (dashed lines) fits. The quadratic relationship has been estimated as a very rough attempt to link simulation points with percolation threshold. For Poisson models, the quadratic relationship is in a smooth continuation with the large-permeability linear relationship, which makes it a plausible trend for low-permeability values. For kinematic models, quadratic and linear trends are very different even for small permeability values, suggesting that the behavior close to the percolation threshold could not follow the classical percolation theory. Note however that it is difficult to draw definite conclusions about the behavior close to the percolation threshold with simulations whose percolation parameters are quite large.

#### 4.2. Flow Distribution Within the Fracture Network

We now analyze the spatial distribution of flow in the DFN structure. We focus especially on the flow channeling, which is commonly observed in natural systems [Abelin et al., 1985], and obviously an important feature of flow for safety assessment. Flow channeling has been mostly studied at the fracture scale [Tsang and Neretnieks, 1998], and barely at the network scale. Considering the simplicity of models at the fracture scale (fractures are assumed hydrologically homogeneous), we do not enter into the detail of flow in the fracture plane. We rather perform a network-scale analysis, where each fracture  $F$  is characterized by a single flow value,  $Q_F$ , which is the total flow exchanged by  $F$  with its neighbors.  $Q_F$  is the half the sum of the absolute values of the flow  $Q_{F,i}$  exchanged through intersections  $i$  (equation (7)).

$$Q_F = \frac{1}{2} \sum_i |Q_{F,i}|, \quad (7)$$

The cumulative distribution of  $Q_F$  is shown in Figure 6. For all curves, we can split fractures in two groups: a first between  $\sim 10^{-3}$  and the maximum flow, which corresponds to fractures well connected to boundaries, and a second lower than  $\sim 10^{-6} - 10^{-4}$ , which corresponds to badly connected fractures. Most of these low-

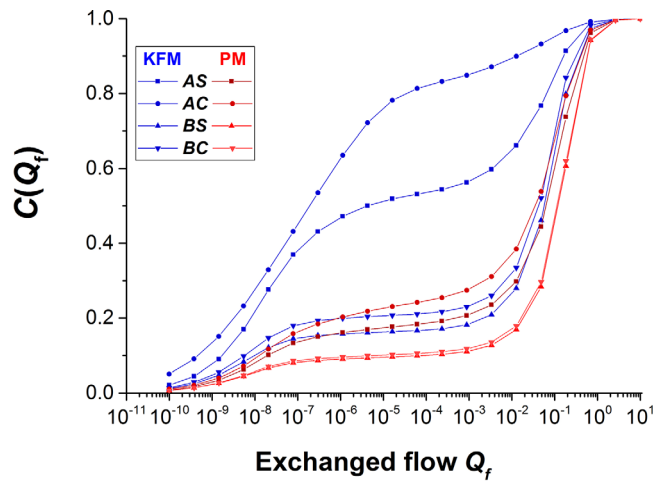
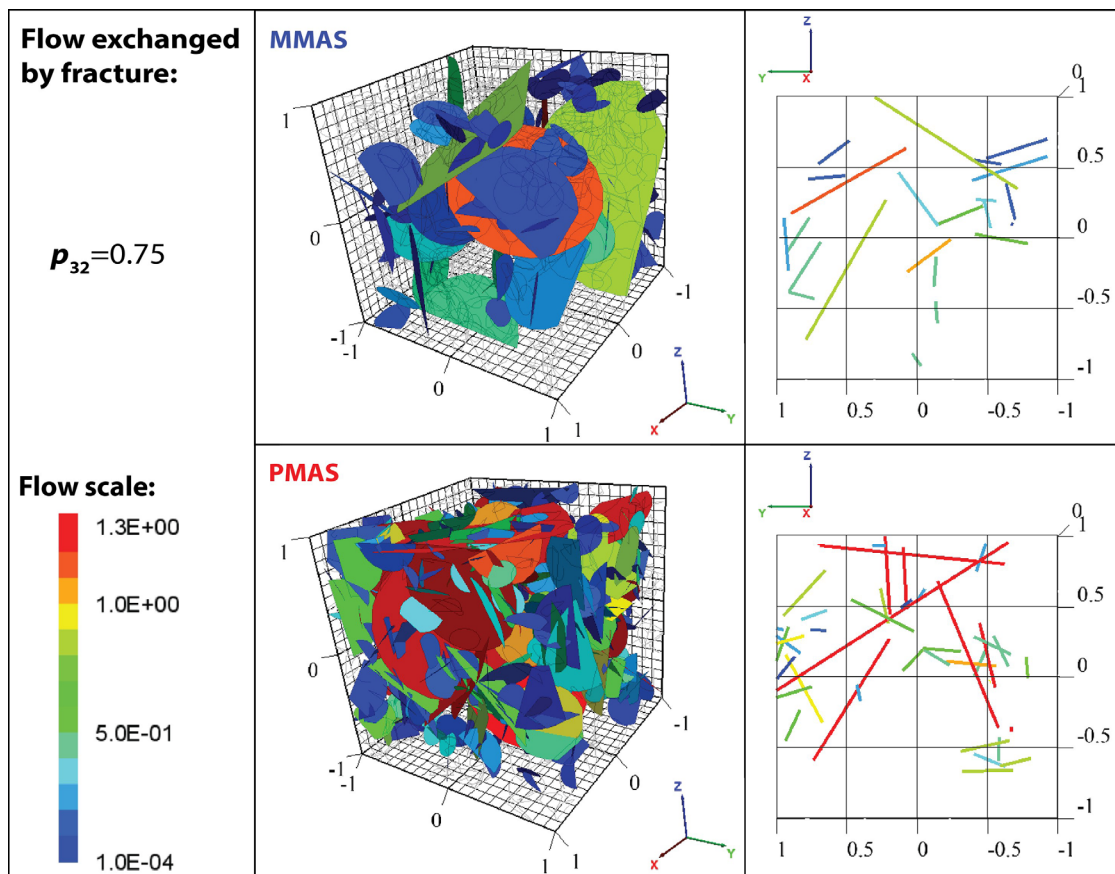


**Figure 6.** Cumulative distribution of  $Q_f$  for both kinematic and Poisson models. Each DFN are symbolized by a symbol, the Poisson DFN are in red, and kinematic models in blue.

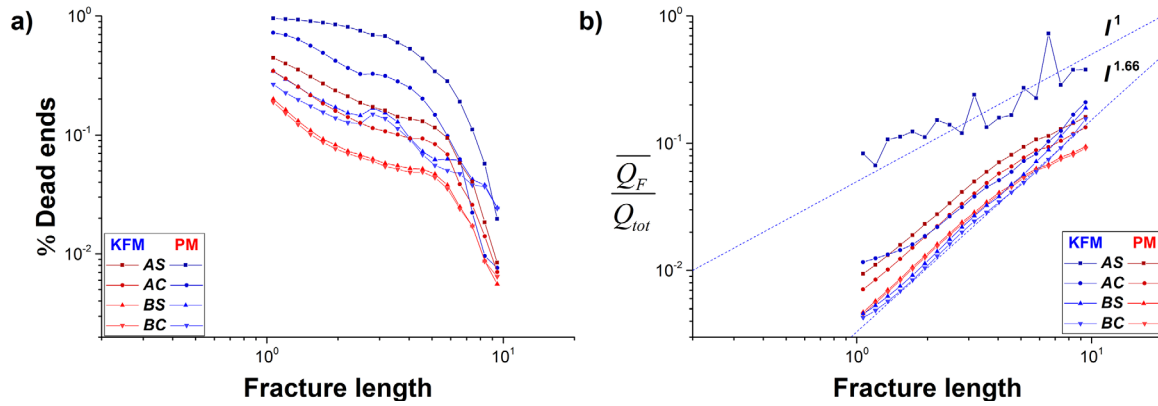
flow fractures are connected by a single intersection to the backbone. In 2-D, these would correspond to dead ends with no flow. In 3-D, a residual flow may exist due to small head gradients along intersection lines. The contribution of these “dead-end” fractures is however negligible. For the high-density models (KFMBC, KFMBS, and all Poisson models), the fractures of the first group (large flow) represent 80% of the total. In contrast to both models MA, where fractures have a single T intersection, this first group is 50% (KFMAC) or even less than 20% (KFMAS), meaning that most of the fractures are dead-ends of flow.

Figure 7 illustrates the DFN flow distribution from both DFN realizations: a KFMAS model, and its equivalent Poisson PMAS. Only fractures in the backbone are shown. Even if both DFN have the same density ( $p_{32}=1.59$ ), the total surface of flowing fractures is significantly smaller in the kinematic model, reflecting the stronger flow channeling of kinematic than of Poisson models. The main differences between both models are (i) the number of main-flow structures (one dominant fracture in KFMAS,

Figure 7 illustrates the DFN flow distribution from both DFN realizations: a



**Figure 7.** (left) Three-dimensional picture and (right) vertical cross section of flow in the (top) sequential kinematic model KFMAS and (bottom) its equivalent Poisson model. Fractures with  $Q_f < 10^{-4}$  are symbolized by an empty disk and other fractures are colored according to their  $Q_f$  value.



**Figure 8.** (a) Average percentage of dead-ends in terms of fracture numbers and (b) average flow in the backbone normalized by total flow for different classes of fracture lengths, i.e., length between  $[l, l+d]$ . For both figures, the averages are calculated for 1000 realizations for each models. The KFM models are in blue and PM in red with symbols indicated in the text box within each plot.

several in PMAS), and (ii) the flow intensity, which is smaller in KFMA than in PMAS (a significant number of fractures in PMAS carries a flow larger than the largest value of KFMA). Both effects contribute to the relatively smaller permeability of kinematic models. Note that the analysis of one particular realization presented in Figure 7 is representative of the average behavior of KFMA models only. For the other kinematic models that are much more connected (KFMB, KFMC, and even KFMA), the flow intensity in the fractures that carry flow is similar to (even slightly larger) the equivalent Poisson models.

Figure 8a shows the percentage of dead-ends (left) and average flow  $\overline{Q}_F(l)$  (right) for the different classes of fracture sizes. For all the models, the percentage of dead-ends is slightly decreasing with  $l$  up to a size of  $\sim 5$ , which is half the system size. Unsurprisingly, the largest percentage of dead-ends is for both kinematic models AC and AS, with up to 3 times more dead-ends than for the equivalent Poisson models, and up to 10 times more than the high-density models (model B and equivalent Poisson). For these latter model, the percentage of dead-ends is rather similar.

Figure 8b shows the average flow per fracture normalized by total flow,  $\theta(l) = \frac{\overline{Q}_F(l)}{Q_t}$ , for different classes of fracture sizes. The analysis is made on all fractures in the backbone (i.e., without dead-ends). The ratio between the total and average flow, i.e.,  $\theta^{-1}$ , is an indicator of the number of independent paths in the system.

For all models but KFMA, the average flow per fracture increases as a power law with fracture length as  $\overline{Q}_F(l) \sim l^{1.66}$ , emphasizing that small fractures contribute to introduce new paths in the system. The average flow and thus the number of paths depend on the model density as expected, and there is not a large difference between kinematic and Poisson models except for fractures larger than half the system size.

The KFMA model is an exception because the average flow per fracture is much higher than in any other model, and because it increases about linearly with fracture length although the trend is characterized by large fluctuations (Figure 8b). KFMA is the model with the smallest density, close to percolation threshold as shown in Figure 5. This may explain why it is so different from the others. Note that the absolute value of the flow  $\overline{Q}_F(l)$  is actually smaller for this model than for the others for all fracture lengths, but the normalization by the total flux per realization in Figure 8b makes  $\frac{\overline{Q}_F(l)}{Q_t}$  larger in Figure 8b.

### 4.3. Backbone

The backbone is the part of fracture network that carries flow. Here we define the backbone in two ways: (i) as the dual of dead-ends defined in section 4.2, i.e., fractures whose flow  $Q_F$  is larger than  $10^{-4}$ , and (ii) by removing iteratively fractures that have only one connection with network or boundaries. Both methods give a similar result. Note that this is not a very restrictive definition since the criteria applies to the whole fracture, independently of the distribution of flow within the fracture plane. A more restrictive criteria based on local flow would end up into a smaller backbone structure.

The backbone density  $d_b$  is a basic measure of the flow structure, worth analyzing when comparing DFN models.  $d_b$  is the sum of the fracture surfaces in backbone divided by the total volume, a definition that makes it directly comparable with  $p_{32}$  (see Table 2 and Figure 9).

**Table 2.** Fracture Densities of the Total DFN ( $p_{32}$ ) and of the Backbone ( $d_b$ ) for KFM and PM DFN

Characteristic	AS	AC	BS	BC
$p_{32}$	1.59 ( $\pm 0.029$ )	1.89 ( $\pm 0.033$ )	2.59 ( $\pm 0.037$ )	2.68 ( $\pm 0.041$ )
$d_b(MM)$	0.29 ( $\pm 0.097$ )	1.17 ( $\pm 0.076$ )	2.19 ( $\pm 0.081$ )	2.42 ( $\pm 0.068$ )
$d_b(PM)$	1.26 ( $\pm 0.05$ )	1.63 ( $\pm 0.035$ )	2.43 ( $\pm 0.02$ )	2.53 ( $\pm 0.02$ )

For the Poisson models, the backbone represents 73–93% of the total fracture density. Similar values are obtained for the kinematic models B (90–95%), but not for model A. The smallest value is for the kinematic model AS, with only 30% of the fracture density belonging to backbone.

Figure 9a shows that  $d_b$  is approximately a linear function of  $p_{32}$ , but the slope and intercept of the fitting functions are different for kinematic and Poisson models. At large  $p_{32}$ , both models converge to 100% of  $p_{32}$ , but large differences are observed for  $p_{32}$  between 1.4 and 2.0. Except for the kinematic model with the largest density (BC), with 95% fractures in the backbone,  $d_b$  is smaller in kinematic than in Poisson models.

In the Figure 9b, we explore the possibility for  $d_b$  to be a first-order control of the bulk permeability. The blue and red curves are linear models with threshold for kinematic and Poisson models, respectively. With the notable exception of the low-density kinematic model KFMA, both linear fits have the same threshold (0.65) but different slopes (0.38 for Poisson models, 0.28 for kinematic models). Thus, the differences in backbone density are not sufficient by themselves to explain the differences in permeability.

#### 4.4. Flow Channeling

The extreme flow channeling often observed in field experiments [Abelin et al., 1990, 1994; Follin et al., 2013; Olsson, 1992] is difficult to replicate with classical Poisson models, and difficult to characterize in 3-D. We use a flow channeling density indicator  $d_Q$ , whose definition is inspired from Davy et al. [1995, 2010] and from the participation ratio in the physics literature [Bell and Dean, 1970; Edwards and Thouless, 1972]:

$$d_Q = \frac{1}{V} \cdot \frac{(\sum_f S_f \cdot Q_f)^2}{(\sum_f S_f \cdot Q_f^2)}, \quad (8)$$

where the surface of fracture  $S_f$  is weighted by the fracture flow  $Q_f$ . The ratio in the right side of equation (8) is a measure of the portion of the total fracture surface, where flow is significant.  $d_Q$  can be directly compared with the fracture density  $p_{32}$ . Its inverse,  $d_Q^{-1}$ , defines the average distance between the main flow paths. It can be related to the average distance between two flowing fractures in a borehole (Figure 10). A small  $d_Q$  corresponds to a large distance between the main flow paths, and thus highly channeled flow at the network scale. Note that  $d_Q$  does not depend on the flow intensity but only on the relative flow distribution (i.e., multiplying the flow distribution by a constant does not change  $d_Q$ ).

Figure 11 shows the relation between  $d_Q$  and  $p_{32}$  (Figure 11a),  $d_Q$  and the percolation parameter  $p$  (Figure 11b), and permeability and  $d_Q$  (Figure 11c) for all DFN models. For both kinematic and Poisson models,  $d_Q$

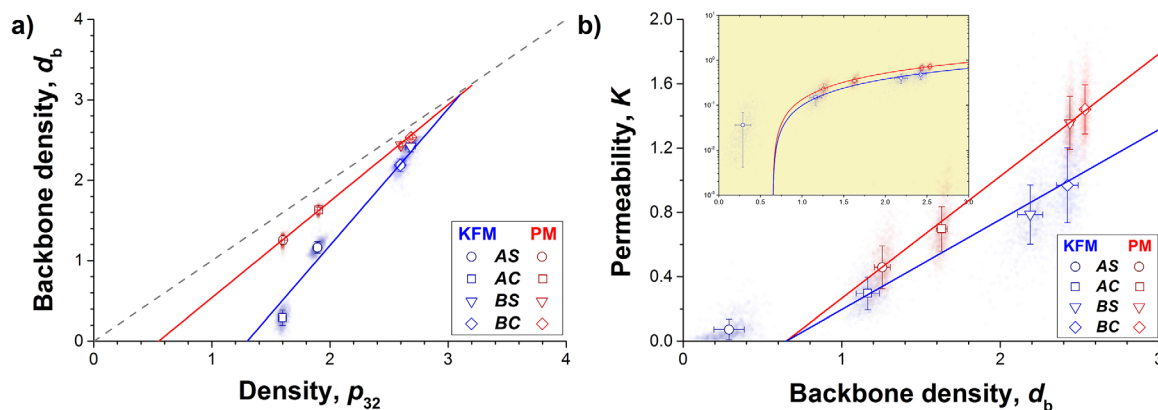


**Figure 9.** (a) Density of the backbone network  $d_b$  as a function of the fracture network density  $p_{32}$ . (b) Relationship between the equivalent permeability and the backbone density  $d_b$ . The yellow box shows the same relationship with log axis.

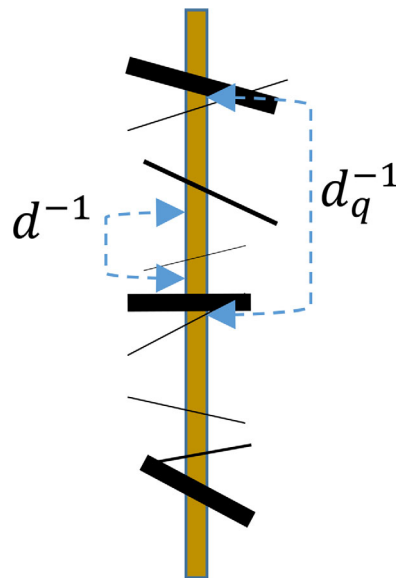


**Figure 10.** Illustration of the fracture and flow distribution along a borehole. Each line symbolizes fracture, and the line thickness symbolizes flow intensity. The average distance of the fracture is the inverse of the fracture density  $d$  (formally  $p_{10}$ ), while the distance between main flow paths is the inverse of the channeling factor  $d_Q$ .  $d_Q$  is necessarily smaller than  $d$ .

increases with  $p_{32}$  but how it does can be interpreted in different ways as discussed below. In any case, the flow channeling density  $d_Q$  of kinematic models is smaller by a factor of 1.5–3 than of Poisson, emphasizing a stronger channeling of the former.

Figure 11b shows that  $d_Q$  is linearly increasing with the percolation parameter  $p$ , and that the intercept of the linear fit at  $d_Q=0$  is the percolation threshold  $p_c$  for both kinematic and Poisson models although the slope of the linear relationship differs between models.  $d_Q$  is thus a proxy for  $p-p_c$ .

Permeability  $K$  is strongly correlated to  $d_Q$  in a relation that does not depend much on the type of model (Figure 11c). A linear relationship is a good fit for most of the large density models (dashed lines in Figure 11c):

$$K = 1.4 (d_Q - 0.25), \quad (9)$$

with the notable exception of the KFMAS model, which is close to the percolation threshold. A quadratic relationship (solid line in Figure 11c) provides a good fit of all models, including KFMAS, especially at low density and permeability:

$$K_{eq} = 1.5 d_Q^2, \quad (10)$$

The linear (dashed line) and quadratic (solid lines) relationships are reported in Figure 11a by combining with equation (6) ( $K$  versus  $p_{32}$  linear relationship shown in Figure 5). The quadratic relationship predicts that  $d_Q$  vanishes with  $K$  as:

$$d_Q = \sqrt{\frac{k}{1.5} (p_{32} - p_{Qc})}, \quad (11)$$

where  $p_{Qc}$  defines the density of fractures that do not contribute significantly to flow. The values of  $k$  and  $p_{Qc}$  depends on the type of model (see discussion in the section following Figure 5), and lead to both blue and red solid lines in Figure 11a. In contrast, a linear relationship  $K$  versus  $d_Q$  would give a linear relationship between  $d_Q$  and  $p_{32}$  (dashed red line in Figure 11a) with a threshold smaller than  $p_{Qc}$ . This would predict a nonnil channeling factor  $d_Q$  around flow threshold.

Although more studies should be done to appraise the behavior of network around threshold of flow, we guess that channeling should be maximum ( $d_Q=0$ ) at threshold, and thus that the quadratic relationship is a solid candidate for the  $K$  versus  $d_Q$  relationship at least for networks close to threshold as KFMAS, independently of the model type.

## 5. Hydraulic Properties for Variable Transmissivity

To complete the comparison between models, we introduce distributions of fracture transmissivities as it is expected in natural systems [Follin *et al.*, 2013; Gustafson and Fransson, 2006; Öhberg and Rouhiainen, 2000; Olsson, 1992]. We restrict this study to (1) a homogenous transmissivity in each fracture, and (2) a lognormal transmissivity distribution uncorrelated to other fracture properties (i.e., fracture length and orientations). As for similar studies [de Dreuzy *et al.*, 2001b], the log-transmissivity distribution is characterized by an average (taken equal to 0, transmissivity of 1) and a dimensionless standard deviation  $\sigma$  taken in the range 0–2.

We plot in Figure 12 both  $K_{eq}$  and  $d_Q$  for different values of  $\sigma$  (kinematic models in Figure 12a, and Poisson models in Figure 12b). For all models, increasing  $\sigma$  leads to an increase of permeability with a decrease of the channeling indicator  $d_Q$ . In other words, systems with a distribution of transmissivity tend to be more efficient and also more channeled than without. However, although the range of  $\sigma$  between 0 and 2 is quite large, the permeability does not change much for all models. Channeling is expected to be a consequence of increasing transmissivity variability [Charlaix *et al.*, 1987; de Dreuzy *et al.*, 2001b]. This effect is observed

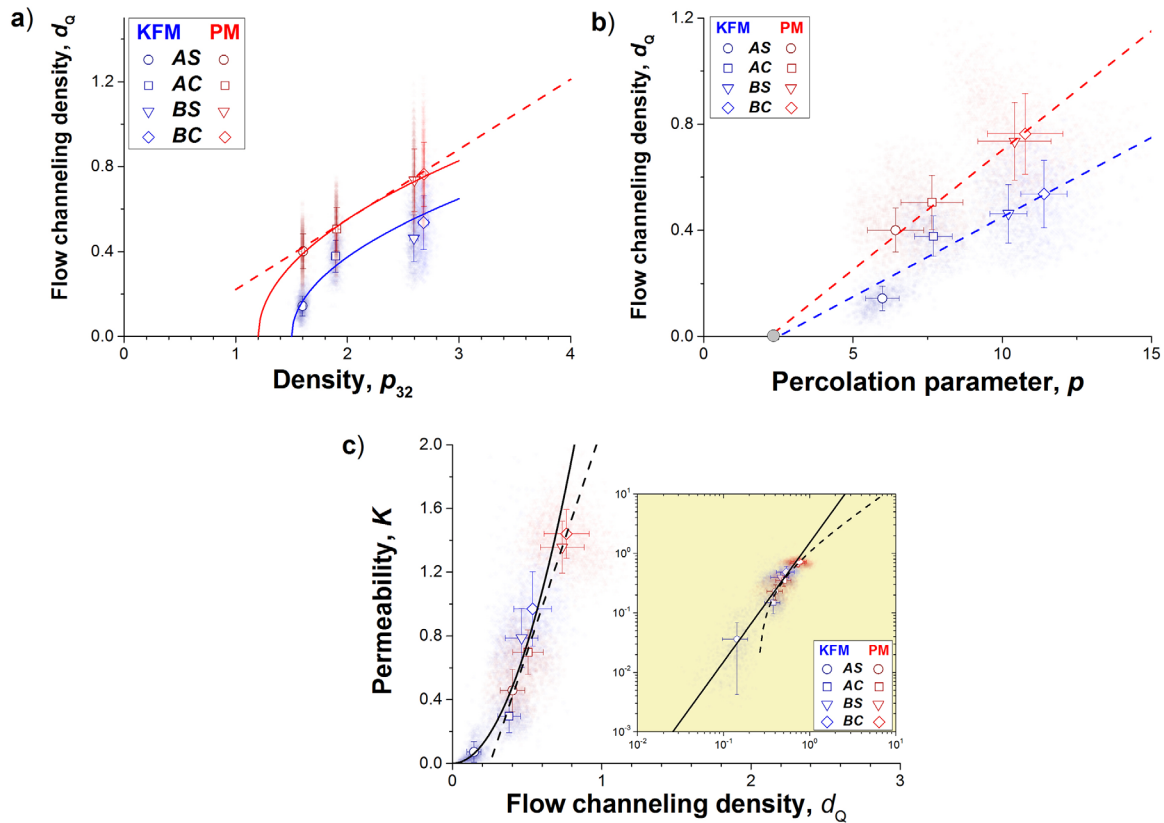


**Figure 11.** Top, channeling factor  $d_Q$  as a function of (a) the density of fracture  $p_{32}$  and (b) the percolation parameter  $p$ . (c) Equivalent permeability as a function of  $d_Q$ . The dashed lines represent linear fits, and the solid lines quadratic fits. Same legends as Figure 5 for symbols.

for all models, but more pronounced for Poisson models than for kinematic ones. It is striking to note that the flow structure is quite insensitive to the transmissivity variability. Moreover, the effects due the DFN structure (Poisson versus kinematic models) remain much larger than those of increasing the variability of transmissivity.

The dependency of flow with  $\sigma$  reflects the flow structure organization. The power average exponent  $\omega$ , defined by  $K_{eq}(\sigma) = K_{eq}(0) \cdot \exp(\omega \cdot \frac{\sigma^2}{2})$ , thus quantifies the flow organization [Desbarats, 1992]:  $\omega$  varies between  $-1$  and  $1$ , and the remarkable values of  $-1$ ,  $0$ , and  $1$  correspond to the harmonic (fractures in

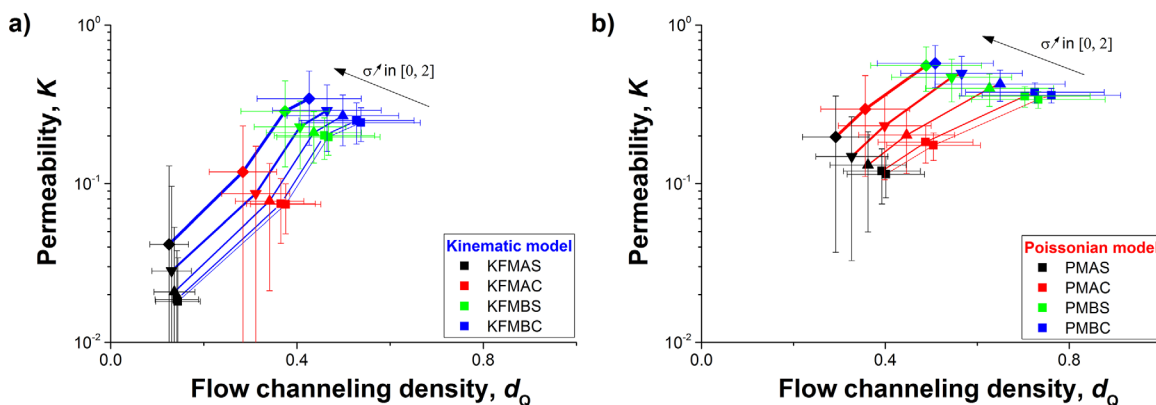


**Figure 12.** Plot of the equivalent permeability transmissivity with respect to the channeling factor for five values of  $\sigma$ , the standard deviation of the log-transmissivity distribution:  $0, 0.5, 1, 1.5,$  and  $2$ . (a) The kinematic models are presented on the left graph and (b) the Poisson models on the right. The thickness of lines symbolizes the value of  $\sigma$ , from the thickest ( $\sigma=2$ ) to the thinnest ( $\sigma=0$ ).

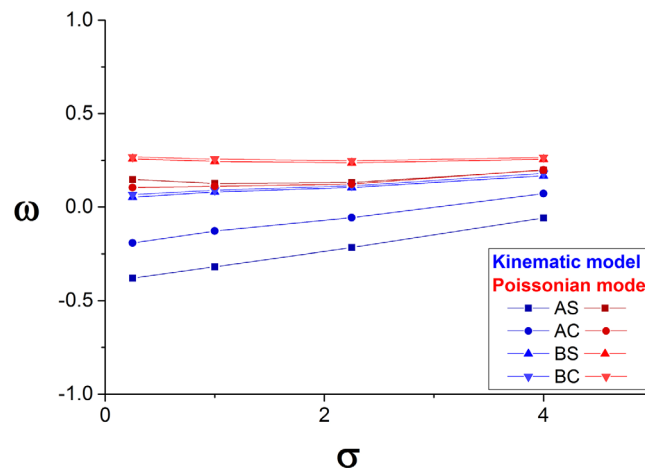


**Figure 13.** Plot of the power average exponent  $\omega$  as a function of  $\sigma^2$ , with  $\sigma$  the standard deviation of the lognormal distribution of fracture transmissivity. The same symbols are used for the different models as in previous figures. Illustration of flow regime is proposed for KFMA5 (in blue) and PMBC (in red) for  $\sigma=0$  and  $\sigma=2$ .

smaller than 0.25, increases with  $\sigma$ , decreases with network density (already observed in *de Dreuzy et al.* [2010]), and are smaller for kinematic model than for their Poisson equivalent.

The decrease of  $\omega$  for the kinematic models highlights an organization with less independent paths, and more fractures in series than for the Poisson models. These configurations are conducive to the existence of bottlenecks for flow as encountered in networks close or slightly above the percolation threshold [*de Dreuzy et al.*, 2010]. Model KFMA5 is particularly sensitive to this critical effect, with  $\omega$  as small as  $-0.45$ .

The fact that  $\omega$  increases with  $\sigma$  can be due to the importance of large structures on flow. Whether they have or not a transmissivity larger or smaller than the average should affect the general flow organization. This effect is hidden by the averaging over all configurations. We plan to address it in a future work.

## 6. Discussion

This study is a first attempt to analyze the consequences of replacing the random (Poisson) hypothesis commonly used to generate DFN by a fracture organization that results from simplified fracturing processes. This model developed by *Davy et al.* [2010, 2013] produces T intersections, as ubiquitously observed in natural fracture networks [*Bonneau et al.*, 2013; *Dahi-Taleghani and Olson*, 2011; *Keshavarzi and Mohammadi*, 2012], and ends up into a hierarchical organization (small fractures abutting large ones) and power law fracture length distributions as commonly observed in natural fracture systems. One main strength of the model is to reproduce these scaling properties from a small set of parameters [*Davy et al.*, 2010].

These kinematic models have been compared with their equivalent Poisson models (same density, length, and orientation distribution, but fractures randomly positioned) for the range of fracture lengths that belongs to the self-similar “dense” regime characterized by a power law fracture length distribution with an exponent of  $-4$ . Different parameters have been used to general models with different dimensionless fracture densities.

The first difference between kinematic and Poisson models is the number of intersections per fracture. For the same density, Poisson models have 1.6–2 times more intersections than kinematic ones, with the same ratio for all the classes of fracture lengths. In addition to the presence of T intersections, this reveals a large difference in fracture organization.

Flow simulations made over more than 1000 realizations per model show significant differences between kinematic models and their Poisson equivalents. The permeability is systematically smaller for kinematic models by a factor 1.5–10. The main difference is that the density of fractures that do not participate in flow is larger in the kinematic models than in their Poisson equivalents.

series), geometric, and arithmetic means (fractures in parallel), respectively. In practice,  $\omega$  is calculated from the following expression [*de Dreuzy et al.*, 2010]:

$$\omega = 2 \cdot \left\langle \frac{\ln \left( \frac{K(\sigma)}{K(0)} \right)}{\ln \left( \frac{T_A}{T_H} \right)} \right\rangle_r, \quad (12)$$

where  $T_A$  and  $T_H$  are the arithmetic and harmonic averages of the fracture transmissivities of the realization  $r$ .  $\omega$  is then obtained by averaging over all realizations [*de Dreuzy et al.*, 2010] (Figure 13). For the two denser Poisson models (PMBC and PMBS),  $\omega$  is independent of  $\sigma$ , and about equal to 0.25, consistent with dense 3-D on-lattice networks studied by *de Dreuzy et al.* [2010]. For all other models,  $\omega$  is

smaller than 0.25, increases with  $\sigma$ , decreases with network density (already observed in *de Dreuzy et al.* [2010]), and are smaller for kinematic model than for their Poisson equivalent.

The decrease of  $\omega$  for the kinematic models highlights an organization with less independent paths, and more fractures in series than for the Poisson models. These configurations are conducive to the existence of bottlenecks for flow as encountered in networks close or slightly above the percolation threshold [*de Dreuzy et al.*, 2010]. Model KFMA5 is particularly sensitive to this critical effect, with  $\omega$  as small as  $-0.45$ .

The fact that  $\omega$  increases with  $\sigma$  can be due to the importance of large structures on flow. Whether they have or not a transmissivity larger or smaller than the average should affect the general flow organization. This effect is hidden by the averaging over all configurations. We plan to address it in a future work.

## 6. Discussion

This study is a first attempt to analyze the consequences of replacing the random (Poisson) hypothesis commonly used to generate DFN by a fracture organization that results from simplified fracturing processes. This model developed by *Davy et al.* [2010, 2013] produces T intersections, as ubiquitously observed in natural fracture networks [*Bonneau et al.*, 2013; *Dahi-Taleghani and Olson*, 2011; *Keshavarzi and Mohammadi*, 2012], and ends up into a hierarchical organization (small fractures abutting large ones) and power law fracture length distributions as commonly observed in natural fracture systems. One main strength of the model is to reproduce these scaling properties from a small set of parameters [*Davy et al.*, 2010].

These kinematic models have been compared with their equivalent Poisson models (same density, length, and orientation distribution, but fractures randomly positioned) for the range of fracture lengths that belongs to the self-similar “dense” regime characterized by a power law fracture length distribution with an exponent of  $-4$ . Different parameters have been used to general models with different dimensionless fracture densities.

The first difference between kinematic and Poisson models is the number of intersections per fracture. For the same density, Poisson models have 1.6–2 times more intersections than kinematic ones, with the same ratio for all the classes of fracture lengths. In addition to the presence of T intersections, this reveals a large difference in fracture organization.

Flow simulations made over more than 1000 realizations per model show significant differences between kinematic models and their Poisson equivalents. The permeability is systematically smaller for kinematic models by a factor 1.5–10. The main difference is that the density of fractures that do not participate in flow is larger in the kinematic models than in their Poisson equivalents.

Another important difference between models is flow channeling. Although this is a striking characteristic feature of geological systems [Berkowitz, 2002; Neuman, 2005; Tsang and Neretnieks, 1998], the intense channeling observed in natural fracture systems is hardly reproduced by Poisson models, except by decreasing fracture density down to the percolation threshold [Follin *et al.*, 2013]. We introduce a measure of channeling  $d_Q$  derived from the participation ratio [Bell and Dean, 1970; Edwards and Thouless, 1972].  $d_Q$  quantifies the actual contribution of the total fracture surface to flow normalized by the system volume.  $d_Q$  is a density, directly comparable (but smaller) to the total fracture density  $p_{32}$ . The smaller is the fracture surface, the higher is the channeling. For Poisson models, flow takes place in a surface that represents about one third to one fourth of the total fracture surfaces. For kinematic models, the ratio is much smaller from one tenth to one fifth.

The kinematic model with the smallest density, KFMAS, differs from the three others as well as from the Poisson models, in the sense that it is an exception for most of the linear trends between permeability and network density (Figures 9b and 11c). This is typical of a behavior close to the percolation threshold, where nonlinear relationships are expected between flow and structure parameters. This is an important issue since small changes in the DFN density parameters can induce large variations of flow properties. The observation that kinematic models tend to produce networks with critical behavior despite percolation parameter well above  $p_c$  has also been reported by [Davy *et al.*, 2010] from 2-D simulations. We note that Poisson and kinematic models do not seem to behave similarly close to percolation threshold, as shown by the relationship between permeability and percolation parameter (Figure 5b).

The kinematic models tend to favor in-series configuration, as shown by the dependency of permeability with transmissivity variations (Figure 13 with negative values of  $\omega$ ), meaning that they will be potentially more sensitive to low-transmissivity fractures than will be the Poisson models. This is still an example of the difference between kinematic and Poisson models, with a behavior potentially more critical for the former than for the latter.

Enhanced channeling is consistent with observations on natural systems. Follin *et al.* [2013] reported that the density of flowing fractures is about 10 times smaller than the density of "open" (i.e., not clogged) fractures in the Forsmark site (Sweden). However, a direct comparison with field data, which is beyond the scope of this study, must address a few issues specific to the adequacy between measures and models:

1. A comparison between model and natural systems requires to fix both the characteristic length  $l_o$  (used for all density terms,  $p_{32}$ ,  $d_Q$ , and  $d_b$ ) and transmissivity  $T_o$  (used for  $K$ ) relevant for natural systems. In Poisson models,  $l_o$  is the lower bound of the power law length distribution, a value hardly known from field measurements. In kinematic models,  $l_o$  is the critical length  $l_c$ , below which fractures are not or badly connected [Davy *et al.*, 2010, 2013]. Darcel *et al.* [2014] estimated  $l_c$  to vary between 1 and 20 m for the Swedish sites of Forsmark, Laxemar, and Simpevarp also studied in Follin *et al.* [2013]. In any case, the actual  $l_o$  value may be very different from the scale at which the fracture density is measured (generally the borehole scale  $\sim 0.1$  m).
2. The channeling measure  $d_Q$  is calculated by characterizing each fracture by a single flow value  $Q_F$ . This is consistent with the assumption of a unique transmissivity value per fracture, but this does not consider potential channeling within the fracture plane that is quite a common phenomenon observed in many field experiments [Abelin *et al.*, 1990, 1994; Neretnieks, 1993; Olsson, 1992], laboratory studies [Birgersson *et al.*, 1993; Brown and Scholz, 1985; Klimczak *et al.*, 2010], and numerical simulations [de Dreuzy *et al.*, 2012; Ishibashi *et al.*, 2012; Tsang and Tsang, 1987].  $d_Q$  is thus an upper bound of the flow density that can be measured at depth in boreholes or in tunnels.
3. Channeling is enhanced by positively correlating transmissivity with fracture length [de Dreuzy *et al.*, 2001b; Frampton and Cvetkovic, 2011; Hyman *et al.*, 2015]. Although the importance of this correlation in natural systems is still an open issue [see, for instance, Follin *et al.*, 2013; Joyce *et al.*, 2014], this effect deserves being tested before deriving conclusions about flow channeling.

Note that only a few parameters of kinematic models have not been deeply investigated in this study. The influence of the domain size  $L$ , of the size of the T intersections, and of potential correlations between transmissivity and fracture length will be the subject of a future study. In a future work, we plan to consider a better description of the fracture nuclei location, which is obviously not a purely uniform random process but should vary as a function of the distance to existing fractures [Bonneau *et al.*, 2016].

## 7. Conclusions

We have analyzed the flow properties of a new DFN model, whose spatial structure results from simplified kinematic rules for fracture nucleation, growth, and arrest. This class of simplified kinematic DFN models are compared with Poisson (i.e., randomly distributed) DFNs with the same geometrical characteristics (same length and orientation distributions, same density). Four kinematic models were designed with different rules of nucleation, growth, and arrest, leading in the dense (i.e., large-scale) regime to power law fracture length distribution with a fixed exponent of  $-4$ , and density terms from 1 to 1.7. In this study, we analyze DFNs with fracture lengths in the dense power law regime only. For all models, the percolation parameter is much larger than the percolation threshold.

In the kinematic models, the number of intersections per fracture smaller by a factor 1.6–2 than in Poisson models. In addition to the presence of T intersections, this reveals one of the main differences in the spatial organization of fracture networks.

For both models, the permeability is well described by a linear relationship with the density  $p_{32}$ , but the threshold (i.e., minimum density to get a nonnil permeability) is 50% larger in kinematic than in Poisson models. The permeability of kinematic models is 1.5–10 times smaller than in Poisson. The largest difference is observed for models with the smallest density, whose  $p_{32}$  is close to threshold.

Both models also differ in the flow organization. Although the backbone (defined in section 4.3) is rather similar for models with the largest densities, it differs significantly for models with the smallest densities, where the number of fractures that participate in flow is significantly smaller in kinematic than in Poisson models.

We calculate a channeling indicator  $d_Q$ , which is a density measure of the surface which transports a significant part of flow.  $d_Q$  is a subset of the total fracture density and even of the backbone density. For Poisson models,  $d_Q$  represents about one third to one fourth of  $p_{32}$ . For kinematic models, the ratio is smaller and varies from one tenth to one fifth, emphasizing an enhanced channeling. Although  $d_Q$  is model dependent, the relationship between permeability  $K$  and  $d_Q$  is likely not, and depends only on the network density. It is quadratic at low densities, and then linear at larger ones.

All the previous results were obtained with a constant transmissivity. We also investigate the sensitivity of permeability and channeling to a distribution of fracture transmissivities (lognormal distributions with standard deviations varying from 0 to 2), and analyze the way permeability averages this distribution. In terms of channeling, kinematic models are less sensitive to transmissivity variability than their Poisson equivalents. The power average exponent  $\omega$ , which quantifies the way averaging proceeds and thus the flow organization, varies between  $-0.5$  and  $\sim 0$  for kinematic models. Such negative values are characteristic of elements in series, rather controlled by small transmissivity values. In contrast,  $\omega$  is slightly positive, between 0.1 and 0.25, for Poisson models, that is between an geometric and arithmetic averaging process.

This analysis demonstrates that choosing an appropriate DFN organization is important for predicting flow properties from fracture network parameters. With the same density, length, and orientation distributions, Poisson models can overestimate permeability by a factor of 10 compared to DFN models built from kinematic rules that mimic the origin of fracturing in geological formations. This is especially true for some of these models with a large number of dead-ends, which behave as systems close to the percolation threshold.

## Appendix A: Number of Intersection Per Fractures

In this appendix, we derive an analytical expression of the number of intersections per fracture  $I_F(I)$ . We first calculate the number of fracture  $F'$  of size  $l'$  that intersect a fracture  $F$  of size  $l$ . This amounts to calculate the volume surrounding  $F$  into which the center of  $F'$  must lie to intersect it. This volume can be approximated by a cylinder of radius  $l+l'/2$ , and height  $\beta l'$ , where  $\beta$  is a coefficient that takes account of the differential orientation of  $F'$  versus  $F$ :

$$V_l = \beta (l+l'/2)^2 \cdot l'$$

The number of fractures in this volume is given by the density of fractures:  $n(l', V) = V \cdot \alpha l'^{-4}$ , as in equation (3), and the total number of intersection is obtained by summing the contribution of all fractures size  $l'$ :

$$n_l(l) = \int_{l'=l_{\min}}^{l'=L} v_{ex} \cdot n(l', L) dl'$$

By using  $p_{32}$  instead of  $\alpha$  ( $p_{32} = \frac{2\alpha}{4} l_{\min}^{-1}$ ), we derive an analytical expression for this integral:

$$n_l(l) = \beta(p_{32} \cdot l_{\min}) \cdot \left( \frac{1}{4} \cdot \log\left(\frac{L}{l_{\min}}\right) + \left(\frac{l}{l_{\min}} - \frac{l}{L}\right) + \frac{1}{2} \left(\frac{l}{l_{\min}}\right)^2 \right) \quad (A1)$$

### Acknowledgments

This work was funded by a Cifre grant ITASCA Consultants SAS/ANRT (Association Nationale Recherche Technologie, France), and partially supported by the Swedish Nuclear Fuel and Waste Management Co. (SKB). The authors are grateful to three anonymous and the Associate Editor for their comments that helped improve the manuscript. We also like to thank Jan-Olof Selroos, Raymond Munier, and Martin Stigsson for constructive discussions and helpful comments. Numerical data and open source codes can be accessed by sending an e-mail to the corresponding author.

### References

- Abelin, H., I. Neretnieks, S. Tunbrant, and L. Moreno (1985), Final report of the migration in a single fracture: Experimental results and evaluation, SKB report, TR 85-03, Svensk Kärnbränslehantering AB, Stockholm.
- Abelin, H., L. Birgersson, and T. Ågren (1990), The channeling experiment-instrumentation and site preparation, SKB report, TR 90-12, Svensk Kärnbränslehantering AB, Stockholm.
- Abelin, H., L. Birgersson, H. Widén, T. Ågren, L. Moreno, and I. Neretnieks (1994), Channeling experiments in crystalline fractured rocks, *J. Contam. Hydrol.*, *15*(3), 129–158.
- Andersson, J., and B. Dverstorp (1987), Conditional simulations of fluid flow in three-dimensional networks of discrete fractures, *Water Resour. Res.*, *23*(10), 1876–1886, doi:10.1029/WR023i10p01876.
- Atkinson, B., and P. Meredith (1987), The theory of subcritical crack growth with applications to minerals and rocks, in *Fracture Mechanics of Rock*, edited by B. K. Atkinson, pp. 111–166, Academic, London, U. K.
- Balberg, I. (1985), Universal percolation-threshold limits in the continuum, *Phys. Rev. B*, *31*(6), 4053–4055.
- Balberg, I. C., H. Anderson, S. Alexander, and N. Wagner (1984), Excluded volume and its relation to the onset of percolation, *Phys. Rev. B*, *30*(7), 3933–3943.
- Bell, R. J., and P. Dean (1970), Atomic vibrations in vitreous silica, *Discuss. Faraday Soc.*, *50*, 55–61, doi:10.1039/DF9705000055.
- Berkowitz, B. (1995), Analysis of fracture network connectivity using percolation theory, *Math. Geol.*, *27*(4), 467–483.
- Berkowitz, B. (2002), Characterizing flow and transport in fractured geological media: A review, *Adv. Water Resour.*, *25*(8), 861–884.
- Birgersson, L., L. Moreno, I. Neretnieks, H. Widén, and T. Ågren (1993), A tracer migration experiment in a small fracture zone in granite, *Water Resour. Res.*, *29*(12), 3867–3878.
- Bonneau, F., V. Henrion, G. Caumon, P. Renard, and J. Sausse (2013), A methodology for pseudo-genetic stochastic modeling of discrete fracture networks, *Comput. Geosci.*, *56*, 12–22, doi:10.1016/j.cageo.2013.02.004.
- Bonneau, F., G. Caumon, and P. Renard (2016), Impact of a stochastic sequential initiation of fractures on the spatial correlations and connectivity of discrete fracture networks, *J. Geophys. Res. Solid Earth*, *121*, 5641–5658, doi:10.1002/2015JB012451.
- Bonnet, E., O. Bour, N. E. Odling, P. Davy, I. Main, P. Cowie, and B. Berkowitz (2001), Scaling of fracture systems in geological media, *Rev. Geophys.*, *39*(3), 347–383, doi:10.1029/1999RG000074.
- Bour, O., and P. Davy (1997), Connectivity of random fault networks following a power law fault length distribution, *Water Resour. Res.*, *33*(7), 1567–1583, doi:10.1029/96WR00433.
- Bour, O., and P. Davy (1998), On the connectivity of three-dimensional fault networks, *Water Resour. Res.*, *34*(10), 2611–2622, doi:10.1029/98WR01861.
- Bour, O., P. Davy, C. Darcel, and N. Odling (2002), A statistical scaling model for fracture network geometry, with validation on a multiscale mapping of a joint network (Hornelen Basin, Norway), *J. Geophys. Res.*, *107*(B6), doi:10.1029/2001JB000176.
- Brown, S. R., and C. H. Scholz (1985), Closure of random elastic surfaces in contact, *J. Geophys. Res.*, *90*(B7), 5531–5545, doi:10.1029/JB090iB07p05531.
- Cacas, M. C., E. Ledoux, G. D. Marsily, A. Barbeau, P. Calmels, B. Gaillard, and R. Magritta (1990a), Modeling fracture flow with a stochastic discrete fracture network: Calibration and validation: 2. The transport model, *Water Resour. Res.*, *26*(3), 491–500.
- Cacas, M. C., E. Ledoux, G. D. Marsily, B. Tillie, A. Barbeau, E. Durand, B. Feuga, and P. Peaudecerf (1990b), Modeling fracture flow with a stochastic discrete fracture network: Calibration and validation: 1. The flow model, *Water Resour. Res.*, *26*(3), 479–489.
- Charlaix, E., E. Guyon, and S. Roux (1987), Permeability of a random array of fractures of widely varying apertures, *Transp. Porous Media*, *2*, 31–43.
- Charles, R. (1958), Dynamic fatigue of glass, *J. Appl. Phys.*, *29*(12), 1657–1662.
- Crampin, S. (1999), Implications of rock criticality for reservoir characterization, *J. Pet. Sci. Eng.*, *24*(1), 29–48.
- Cvetkovic, V., S. Painter, N. Outters, and J. O. Selroos (2004), Stochastic simulation of radionuclide migration in discretely fractured rock near the Äspö Hard Rock Laboratory, *Water Resour. Res.*, *40*, W02404, doi:10.1029/2003WR002655.
- Dahi-Taleghani, A., and J. E. Olson (2011), Numerical modeling of multistranded-hydraulic-fracture propagation: Accounting for the interaction between induced and natural fractures, *SPE J.*, *16*(03), 575–581.
- Darcel, C., O. Bour, P. Davy, and J. R. D. Dreuzy (2003), Connectivity properties of two-dimensional fracture networks with stochastic fractal correlation, *Water Resour. Res.*, *39*(10), 1272, doi:10.1029/2002WR001628.
- Darcel, C., R. Le Goc, P. Davy, and I. Olofsson (2014), Including variability into a quantitative DFN modeling approach—Application to SKB sites, paper presented at 1st International Conference on Discrete Fracture Network Engineering DFNE 2014, Canadian Rock Mechanics Association (CARMA), Vancouver, British Columbia, Canada.
- Davy, P. (1993), On the frequency-length distribution of the San Andreas Fault System, *J. Geophys. Res.*, *98*(B7), 12,141–12,151, doi:10.1029/93JB00372.
- Davy, P., A. Sornette, and D. Sornette (1990), Some consequences of a proposed fractal nature of continental faulting, *Nature*, *348*(6296), 56–58, doi:10.1038/348056a0.
- Davy, P., A. Hansen, E. Bonnet, and S.-Z. Zhang (1995), Localization and fault growth in layered brittle-ductile systems: Implications for deformations of the continental lithosphere, *J. Geophys. Res.*, *100*(B4), 6281–6294, doi:10.1029/94JB02983.
- Davy, P., O. Bour, J. R. De Dreuzy, and C. Darcel (2006), Flow in multiscale fractal fracture networks, in *Fractal Analysis for Natural Hazards*, edited by G. Cello and B. D. Malamud, pp. 31–45, Geol. Soc. Publ., Bath, U. K.
- Davy, P., R. Le Goc, C. Darcel, O. Bour, J.-R. de Dreuzy, and R. Munier (2010), A likely universal model of fracture scaling and its consequence for crustal hydromechanics, *J. Geophys. Res.*, *115*, B10411, doi:10.1029/2009JB007043.

- Davy, P., R. Le Goc, and C. Darcel (2013), A model of fracture nucleation, growth and arrest, and consequences for fracture density and scaling, *J. Geophys. Res. Solid Earth*, *118*, 1393–1407, doi:10.1002/jgrb.50120.
- de Dreuzy, J.-R., P. Davy, and O. Bour (2000), Percolation parameter and percolation-threshold estimates for three-dimensional random ellipses with widely scattered distributions of eccentricity and size, *Phys. Rev. E*, *62*(5), 5948–5952.
- de Dreuzy, J.-R., P. Davy, and O. Bour (2001a), Hydraulic properties of two-dimensional random fracture networks following a power law length distribution: 1. Effective connectivity, *Water Resour. Res.*, *37*(8), 2065–2078, doi:10.1029/2001WR900011.
- de Dreuzy, J.-R., P. Davy, and O. Bour (2001b), Hydraulic properties of two-dimensional random fracture networks following a power law length distribution: 2. Permeability of networks based on lognormal distribution of apertures, *Water Resour. Res.*, *37*(8), 2079–2096, doi:10.1029/2001WR900010.
- de Dreuzy, J.-R., P. Davy, and O. Bour (2002), Hydraulic properties of two-dimensional random fracture networks following power law distributions of length and aperture, *Water Resour. Res.*, *38*(12), 1276, doi:10.1029/2001WR001009.
- de Dreuzy, J.-R., P. D. Boiry, G. Pichot, and P. Davy (2010), Use of power averaging for quantifying the influence of structure organization on permeability upscaling in on-lattice networks under mean parallel flow, *Water Resour. Res.*, *46*, W08519, doi:10.1029/2009WR008769.
- de Dreuzy, J.-R., Y. Méheust, and G. Pichot (2012), Influence of fracture scale heterogeneity on the flow properties of three-dimensional discrete fracture networks (DFN), *J. Geophys. Res.*, *117*, B11207, doi:10.1029/2012JB009461.
- De Dreuzy, J.-R., G. Pichot, B. Poirriez, and J. Erhel (2013), Synthetic benchmark for modeling flow in 3D fractured media, *Comput. Geosci.*, *50*, 59–71.
- Dershowitz, W., and H. Einstein (1988), Characterizing rock joint geometry with joint system models, *Rock Mech. Rock Eng.*, *21*(1), 21–51.
- Dershowitz, W. S., and H. H. Herda (1992), Interpretation of fracture spacing and intensity, paper presented at Rock Mechanics, Balkema, Rotterdam, Netherlands.
- Desbarats, A. J. (1992), Spatial averaging of hydraulic conductivity in three-dimensional heterogeneous porous media, *Math. Geol.*, *24*(3), 249–267.
- Edwards, J. T., and D. J. Thouless (1972), Numerical studies of localization in disordered systems, *J. Phys. C*, *5*(8), 807–820.
- Erhel, J., J. de Dreuzy, and B. Poirriez (2009a), Flow simulation in three-dimensional discrete fracture networks, *SIAM J. Sci. Comput.*, *31*(4), 2688–2705, doi:10.1137/080729244.
- Erhel, J., J. R. De Dreuzy, and B. Poirriez (2009b), Flow simulation in three-dimensional discrete fracture networks, *SIAM J. Sci. Comput.*, *31*(4), 2688–2705, doi:10.1137/080729244.
- Follin, S., L. Hartley, I. Rhén, P. Jackson, S. Joyce, D. Roberts, and B. Swift (2013), A methodology to constrain the parameters of a hydrogeological discrete fracture network model for sparsely fractured crystalline rock, exemplified by data from the proposed high-level nuclear waste repository site at Forsmark, Sweden, *Hydrogeol. J.*, *22*(2), 313–331, doi:10.1007/s10040-013-1080-2.
- Frampton, A., and V. Cvetkovic (2011), Numerical and analytical modeling of advective travel times in realistic three-dimensional fracture networks, *Water Resour. Res.*, *47*, W02506, doi:10.1029/2010WR009290.
- Gudmundsson, A. (1987), Geometry, formation and development of tectonic fractures on the Reykjanes Peninsula, southwest Iceland, *Tectonophysics*, *139*(3), 295–308.
- Gustafson, G., and Å. S. Fransson (2006), The use of the Pareto distribution for fracture transmissivity assessment, *Hydrogeol. J.*, *14*(1-2), 15–20, doi:10.1007/s10040-005-0440-y.
- Hardebol, N. J., C. Maier, H. Nick, S. Geiger, G. Bertotti, and H. Boro (2015), Multiscale fracture network characterization and impact on flow: A case study on the Latemar carbonate platform, *J. Geophys. Res. Solid Earth*, *120*, 8197–8222, doi:10.1002/2015JB011879.
- Hsieh, P. A. (1998), Scale effects in fluid flow through fractured geological media, in *Scale Dependence and Scale Invariance in Hydrology*, edited by G. Sposito, pp. 335–353, Cambridge Univ. Press, Cambridge.
- Hyman, J. D., S. L. Painter, H. Viswanathan, N. Makedonska, and S. Karra (2015), Influence of injection mode on transport properties in kilometer-scale three-dimensional discrete fracture networks, *Water Resour. Res.*, *51*, 7289–7308, doi:10.1002/2015WR017151.
- Ishibashi, T., N. Watanabe, N. Hirano, A. Okamoto, and N. Tsuchiya (2012), GeoFlow: A novel model simulator for prediction of the 3-D channeling flow in a rock fracture network, *Water Resour. Res.*, *48*, W07601, doi:10.1029/2011WR011226.
- Jing, L., and O. Stephansson (2007), Discrete Fracture Network (DFN) method, in *Developments in Geotechnical Engineering*, edited by J. Lanru and S. Ove, pp. 365–398, Elsevier, Amsterdam, Netherlands.
- Joyce, S., L. Hartley, D. Applegate, J. Hoek, and P. Jackson (2014), Multi-scale groundwater flow modeling during temperate climate conditions for the safety assessment of the proposed high-level nuclear waste repository site at Forsmark, Sweden, *Hydrogeol. J.*, *22*(6), 1233–1249, doi:10.1007/s10040-014-1165-6.
- Kerrou, J., P. Renard, H.-J. Hendricks Franssen, and I. Lunati (2008), Issues in characterizing heterogeneity and connectivity in non-multiGaussian media, *Adv. Water Resour.*, *31*(1), 147–159, doi:10.1016/j.advwatres.2007.07.002.
- Keshavarzi, R., and S. Mohammadi (2012), A new approach for numerical modeling of hydraulic fracture propagation in naturally fractured reservoirs, paper presented at SPE/EAGE European Unconventional Resources Conference and Exhibition, 20–22 March, Vienna, Austria.
- Kirkpatrick, S. (1973), Percolation and Conduction, *Rev. Modern Phys.*, *45*(4), 574–588.
- Klimczak, C., R. Schultz, R. Parashar, and D. Reeves (2010), Cubic law with aperture-length correlation: Implications for network scale fluid flow, *Hydrogeol. J.*, *18*(4), 851–862, doi:10.1007/s10040-009-0572-6.
- Knudby, C., and J. Carrera (2005), On the relationship between indicators of geostatistical, flow and transport connectivity, *Adv. Water Resour.*, *28*(4), 405–421.
- Le Goc, R., J. R. de Dreuzy, and P. Davy (2010), Statistical characteristics of flow as indicators of channeling in heterogeneous porous and fractured media, *Adv. Water Resour.*, *33*(3), 257–269, doi:10.1016/j.advwatres.2009.12.002.
- Long, J. C. S., and D. Billaux (1987), From field data to fracture network modeling: An example incorporating spatial structure, *Water Resour. Res.*, *23*(7), 1201–1216.
- Long, J. C. S., J. S. Remer, C. R. Wilson, and P. A. Witherspoon (1982), Porous media equivalents for networks of discontinuous fractures, *Water Resour. Res.*, *18*(3), 645–658.
- Long, J. C. S., P. Gilmour, and P. A. Witherspoon (1985), A model for steady fluid flow in random three-dimensional networks of disc-shaped fractures, *Water Resour. Res.*, *21*(8), 1105–1115.
- Margolin, G., B. Berkowitz, and H. Scher (1998), Structure, flow, and generalized conductivity scaling in fracture networks, *Water Resour. Res.*, *34*(9), 2103–2121.
- Martinez-Landa, L., and J. Carrera (2005), An analysis of hydraulic conductivity scale effects in granite (Full-scale Engineered Barrier Experiment (FEBEX), Grimsel, Switzerland), *Water Resour. Res.*, *41*, W03006, doi:10.1029/2004WR003458.
- McClure, M., and R. N. Horne (2013), *Discrete Fracture Network Modeling of Hydraulic Stimulation: Coupling Flow and Geomechanics*, Springer, New York.

- Mitescu, C. D., and M. J. Musolf (1983), Critical exponent for 3-D percolation conductivity, revisited, *J. Phys. Lett.*, *44*(16), 679–683, doi:10.1051/jphyslet:019830044016067900.
- Nakaya, S., and K. Nakamura (2007), Percolation conditions in fractured hard rocks: A numerical approach using the three-dimensional binary fractal fracture network (3D-BFFN) model, *J. Geophys. Res.*, *112*, B12203, doi:10.1029/2006JB004670.
- Neretnieks, I. (1993), Solute transport in fractured rock—Applications to radionuclide waste repositories, in *Flow and Contaminant Transport in Fractured Rock*, edited by J. Bear et al., pp. 39–127, Academic Press, Inc., San Diego, Calif.
- Neuman, S. (2005), Trends, prospects and challenges in quantifying flow and transport through fractured rocks, *Hydrogeol. J.*, *13*(1), 124–147, doi:10.1007/s10040-004-0397-2.
- Oda, M. (1985), Permeability tensor for discontinuous rock masses, *Géotechnique*, *35*(4), 483–495, doi:10.1680/geot.1985.35.4.483.
- Odling, N. E. (1997), Scaling and connectivity of joint systems in sandstones from western Norway, *J. Struct. Geol.*, *19*(10), 1257–1271, doi:10.1016/S0191-8141(97)00041-2.
- Öhberg, A., and P. Rouhiainen (2000), *Posiva Groundwater Flow Measuring Techniques*, Posiva Oy, Helsinki.
- Olsson, O. (1992), Site characterization and validation, final report, Stripa Project TR 92-22, Svensk Kärnbränslehantering AB, Stockholm.
- Park, Y.-J., J.-R. D. Dreuzy, K.-K. Lee, and B. Berkowitz (2001), Transport and intersection mixing in random fracture networks with power law length distributions, *Water Resour. Res.*, *37*(10), 2493–2501.
- Poisson, S. D. (1837), *Recherches Sur la Probabilité des Jugements en Matière Criminelle et en Matière Civile*, Bachelier, Paris.
- Renshaw, C. E. (1999), Connectivity of joint networks with power law length distributions, *Water Resour. Res.*, *35*(9), 2661–2670, doi:10.1029/1999WR900170.
- Ronayne, M. J., and S. M. Gorelick (2006), Effective permeability of porous media containing branching channel networks, *Phys. Rev. E*, *73*(2), 026305.
- Sanderson, D. J., and C. W. Nixon (2015), The use of topology in fracture network characterization, *J. Struct. Geol.*, *72*, 55–66, doi:10.1016/j.jsg.2015.01.005.
- Scheibe, T., and S. Yabusaki (1998), Scaling of flow and transport behavior in heterogeneous groundwater systems, *Adv. Water Resour.*, *22*(3), 223–238.
- Scholz, C. H., and P. A. Cowie (1990), Determination of total strain from faulting using slip measurements, *Nature*, *346*, 837–839.
- Segall, P., and D. D. Pollard (1983), Joint formation in granitic rock of the Sierra Nevada, *Geol. Soc. Am. Bull.*, *94*(5), 563–575, doi:10.1130/0016-7606.
- Selroos, J.-O., D. D. Walker, A. Ström, B. Gylling, and S. Follin (2002), Comparison of alternative modelling approaches for groundwater flow in fractured rock, *J. Hydrol.*, *257*(1–4), 174–188, doi:10.1016/S0022-1694(01)00551-0.
- Stauffer, D., and A. Aharony (1992), *Introduction to Percolation Theory*, 2nd ed., Taylor and Francis, Bristol, U. K.
- Trincherro, P., X. Sánchez-Vila, and D. Fernández-García (2008), Point-to-point connectivity, an abstract concept or a key issue for risk assessment studies?, *Adv. Water Resour.*, *31*(12), 1742–1753.
- Tsang, C.-F., and I. Neretnieks (1998), Flow channeling in heterogeneous fractured rocks, *Rev. Geophys.*, *36*(2), 275–298, doi:10.1029/97RG03319.
- Tsang, Y. W., and C. Tsang (1987), Channel model of flow through fractured media, *Water Resour. Res.*, *23*(3), 467–479.
- Turcotte, D. L. (1986), A fractal model for crustal deformation, *Tectonophysics*, *132*, 261–269.
- Wellman, T. P., A. M. Shapiro, and M. C. Hill (2009), Effects of simplifying fracture network representation on inert chemical migration in fracture-controlled aquifers, *Water Resour. Res.*, *45*, W01416, doi:10.1029/2008WR007025.